

Fine structure of exciton excited levels in a quantum dot with a magnetic ion

M.M. Glazov, E.L. Ivchenko

A.F. Ioffe Physico-Technical Institute, Russian Academy of Sciences, 194021 St.-Petersburg, Russia

L. Besombes, Y. Léger, L. Maingault and H. Mariette

CEA-CNRS group "Nanophysique et Semiconducteurs", Laboratoire de spectrométrie physique, CNRS and Université Joseph Fourier-Grenoble 1, BP 87, F-38402 St Martin d'Hères, France

The fine structure of excited excitonic states in a quantum dot with an embedded magnetic ion is studied theoretically and experimentally. The developed theory takes into account the Coulomb interaction between charged carriers, the anisotropic long-range electron-hole exchange interaction in the zero-dimensional exciton, and the exchange interaction of the electron and the hole with the d -electrons of a Mn ion inserted inside the dot. Depending on the relation between the quantum dot anisotropy and the exciton-Mn coupling the photoluminescence excitation spectrum has a qualitatively different behavior. It provides a deep insight into the spin structure of the excited excitonic states.

I. INTRODUCTION

Optical microspectroscopy is a set of powerful optical techniques that do not damage the sample and allow one to extract local quantitative information on micron and submicron scales. These high spatial resolution optical techniques has been used to measure the photoluminescence (PL) from single quantum dots and study the exchange interaction between a zero-dimensional exciton and a few^{1,2} or a single magnetic ion embedded in the quantum dots (QD)^{3,4,5,6,7}. Theoretically, the ground state energy spectrum of a quantum dot containing a Mn ion was studied in Refs. 8,9,10.

In this work we have theoretically and experimentally studied the fine structure of *excited* excitonic states in such magnetically-doped QDs. We have developed a theory taking into account both direct Coulomb and long-range exchange interaction between an electron and a hole in the zero-dimensional exciton and exchange interaction of the coupled electron-hole pair with the Mn d -electrons. The fine structure of the excited state is shown to be determined by an interplay of the anisotropic electron-hole long-range exchange interaction, Coulomb interaction between the charge carriers and the coupling of an exciton with a Mn ion.

The developed theory is compared with the PL excitation (PLE) measurements on an individual QD carrying a Mn²⁺ ion. The coupling constants of exciton-Mn interaction for the ground and optically active excited states are determined. The analysis of the fine structure of the excited states allows us to determine the degree of QD anisotropy and make conclusions about the magnetic ion position in a quantum dot.

The paper is organized in a following way: Sec. II is devoted to the theoretical analysis of the fine structure of pp -shell excitonic states in the QD without a Mn ion, Sec. III presents the results on the exciton interaction with the magnetic ion, and Sec. IV presents the experimental results and their analysis.

II. EXCITON STATES IN NON-MAGNETIC DOTS

We consider heavy-hole exciton states in a single quantum-well quantum dot. This means that we neglect heavy-light hole mixing and assume an exciton to be formed by a conduction-band electron with the spin $s = \pm 1/2$ and a heavy hole with the spin (or angular-momentum component) $j = \pm 3/2$.⁶ For the in-plane confinement of free carriers, we choose *coaxial parabolic* potentials with z as the principal axis. In what follows we concentrate on QDs of sizes small enough to have the in-plane localization lengths for electrons (a_e) or holes (a_h) smaller than the two-dimensional (2D) exciton Bohr radius a_B .

To begin with, let us consider an axially (cylindrically) symmetric QD where the exciton ground state (ss -shell) is described by the envelope

$$S(\rho_e, \rho_h) = \frac{1}{\pi a_e a_h} \exp\left(-\frac{\rho_e^2}{2a_e^2} - \frac{\rho_h^2}{2a_h^2}\right), \quad (1)$$

where $\rho_{e,h}$ is the electron or hole in-plane radius vector with the components x_e, y_e or x_h, y_h referred to the center of the confining potential. Similarly, the pp -orbital excited states being the products of electron and hole $P_{x,y}$ orbitals have the form

$$\begin{aligned} D_{xx}(\rho_e, \rho_h) &= 2 \frac{x_e x_h}{a_e a_h} S(\rho_e, \rho_h), & D_{yy}(\rho_e, \rho_h) &= 2 \frac{y_e y_h}{a_e a_h} S(\rho_e, \rho_h), \\ D_{xy}(\rho_e, \rho_h) &= 2 \frac{x_e y_h}{a_e a_h} S(\rho_e, \rho_h), & D_{yx}(\rho_e, \rho_h) &= 2 \frac{y_e x_h}{a_e a_h} S(\rho_e, \rho_h), \end{aligned} \quad (2)$$

where the subscripts in D_{xx} , D_{yy} , D_{xy} , and D_{yx} describe the symmetry of the P -orbitals for an electron and a hole.

In the isotropic parabolic potential the four pp -shell states are degenerate. The Coulomb interaction between an electron and a hole lifts this degeneracy, see Fig. 1a. The lowest lying state with the wavefunction

$$|1\rangle = \frac{1}{\sqrt{2}} [D_{xx}(\boldsymbol{\rho}_e, \boldsymbol{\rho}_h) + D_{yy}(\boldsymbol{\rho}_e, \boldsymbol{\rho}_h)] \quad (3)$$

is optically active. The states $|2\rangle = [D_{xx}(\boldsymbol{\rho}_e, \boldsymbol{\rho}_h) - D_{yy}(\boldsymbol{\rho}_e, \boldsymbol{\rho}_h)]/\sqrt{2}$ and $|3\rangle = [D_{xy}(\boldsymbol{\rho}_e, \boldsymbol{\rho}_h) + D_{yx}(\boldsymbol{\rho}_e, \boldsymbol{\rho}_h)]/\sqrt{2}$ are degenerate and they are shifted above the state $|1\rangle$ by the energy

$$V_C = \frac{3\sqrt{\pi}}{4} \frac{\zeta^2}{(1 + \zeta^2)^{5/2}} \frac{e^2}{\varkappa_0 a_e}, \quad (4)$$

where \varkappa_0 is the low-frequency dielectric constant and $\zeta = a_h/a_e$. The splitting between the pair of states $|2\rangle$, $|3\rangle$ and the highest state $|4\rangle = [D_{xy}(\boldsymbol{\rho}_e, \boldsymbol{\rho}_h) - D_{yx}(\boldsymbol{\rho}_e, \boldsymbol{\rho}_h)]/\sqrt{2}$ is given by V_C as well. The binding energy of the exciton $|1\rangle$ referred to the unperturbed position of pp -orbitals reads

$$E_b = \frac{\sqrt{\pi}}{2} \frac{\zeta^4 + 5\zeta^2 + 1}{(1 + \zeta^2)^{5/2}} \frac{e^2}{\varkappa_0 a_e}. \quad (5)$$

The parameters E_b and V_C completely determine the direct Coulomb interaction in the parabolic QD.

We next turn to the slightly elliptical QD where the effective localization radii a_e and a_h are replaced by localization lengths $a_{e,i}$, $a_{h,i}$ ($i = x, y$) in the x and y directions. The anisotropy is characterized by the ratios

$$\beta_e = \frac{a_{e,y} - a_{e,x}}{2a_e}, \quad \beta_h = \frac{a_{h,y} - a_{h,x}}{2a_h}.$$

For simplicity we assume $\beta_e = \beta_h \equiv \beta$ and $\beta \ll 1$. The anisotropy fully lifts the degeneracy of pp -orbital states. In the case of large anisotropy (the criterion is given below) the splitting between two bright states $D_{xx}(\boldsymbol{\rho}_e, \boldsymbol{\rho}_h)$ and $D_{yy}(\boldsymbol{\rho}_e, \boldsymbol{\rho}_h)$ is given (to the lowest order in β) by

$$E_a = E_{xx} - E_{yy} = \left(1 + \frac{\sigma}{\zeta^2}\right) \frac{4\hbar^2\beta}{m_e a_e^2}, \quad (6)$$

where $\sigma = m_e/m_h$ characterizes electron-hole mass ratio. The splitting between the dark states, $D_{xy}(\boldsymbol{\rho}_e, \boldsymbol{\rho}_h)$ and $D_{yx}(\boldsymbol{\rho}_e, \boldsymbol{\rho}_h)$, arises due to the difference between carrier masses and/or localization radii, namely,

$$E'_a = E_{xy} - E_{yx} = \left(1 - \frac{\sigma}{\zeta^2}\right) \frac{4\hbar^2\beta}{m_e a_e^2}. \quad (7)$$

The transition between the Coulomb-dominated and anisotropy-dominated regimes takes place at $|E_a| \sim V_C$.

The long-range exchange interaction affecting the bright exciton with $m = \pm 1$ is described by^{11,12}

$$\mathcal{H}_{n'n}^{(\text{long})} = \frac{1}{4\pi\varkappa_\infty} \left(\frac{e\hbar|p_0|}{m_0 E_g}\right)^2 \int d\mathbf{K} \frac{K_{m'}^* K_m}{K} \tilde{\psi}_{n'}^*(\mathbf{K}) \tilde{\psi}_n(\mathbf{K}), \quad (8)$$

where n (or n') is the exciton-state index including both the angular-momentum component m (or m') and orbital state, \varkappa_∞ is the high-frequency dielectric constant, \mathbf{K} is the two-dimensional center of mass wave vector with the components $K_x, K_y, K_{\pm 1} = K_x \pm iK_y$, m_0 is the free electron mass, E_g is the band gap, p_0 is the interband matrix element of the momentum operator, and we introduced the 2D Fourier-transform $\tilde{\psi}(\mathbf{K}) = \int d\boldsymbol{\rho} e^{-i\mathbf{K}\boldsymbol{\rho}} \Psi(\boldsymbol{\rho}, \boldsymbol{\rho})$ of the exciton envelope function $\Psi(\boldsymbol{\rho}_e, \boldsymbol{\rho}_h)$ taken at the coinciding coordinates, $\boldsymbol{\rho}_e = \boldsymbol{\rho}_h \equiv \boldsymbol{\rho}$. For the ss -shell, $\Psi_n(\boldsymbol{\rho}, \boldsymbol{\rho}) = S(\boldsymbol{\rho}, \boldsymbol{\rho})$ and, for the pp -shell states $|D_{\alpha\beta}, m\rangle$, $\Psi_n(\boldsymbol{\rho}, \boldsymbol{\rho}) = D_{\alpha\beta}(\boldsymbol{\rho}, \boldsymbol{\rho})$ with α and β running through x, y .

In the isotropic QD the ss -shell radiative doublet is not split by the interaction long-range interaction Eq. (8). We introduce the characteristic value of the long-range exchange for pp -shell states

$$\mathcal{E} = \left(\frac{e\hbar|p_0|}{m_0 E_g}\right)^2 \frac{\sqrt{\pi}}{16\varkappa_\infty a_e^3 \zeta \sqrt{1 + \zeta^2}}. \quad (9)$$

For CdTe QD with $a_e = 45 \text{ \AA}$, $a_h = 90 \text{ \AA}$, $\varkappa_0 = 10.4$, $\varkappa_\infty = 7.1$, $2p_0^2/m_0 = 17.9 \text{ eV}$, $E_g = 1.6 \text{ eV}$ [see Ref. 11] the Coulomb interaction induced splitting $V_C \sim 3 \text{ meV}$ and $\mathcal{E} \sim 1.5 \times 10^{-2} \text{ meV}$. Thus, $\mathcal{E} \ll V_C$ and the exchange interaction should be considered as a correction to the direct Coulomb interaction.¹⁸ Therefore, in an axial QD the exchange-induced splitting of the radiative pp -orbital doublet is proportional to \mathcal{E}^2/V_C and can be neglected.

If the QD possesses an anisotropy in the axes x, y the radiative doublet of the ground state (1) is split into a pair of linearly polarized sublevels with the microscopic dipole momentum parallel to x and y . This anisotropic splitting is given by

$$\delta E_s = 24\beta\mathcal{E}, \quad (10)$$

and is proportional to the anisotropy degree β entering also into Eqs. (6), (7). If anisotropic splitting, E_a , of the pp -shells D_{xx} , D_{yy} exceeds the Coulomb energy V_C , each shell is additionally split into radiative sublevels $|D_{xx}, x\rangle, |D_{xx}, y\rangle$ or $|D_{yy}, x\rangle, |D_{yy}, y\rangle$ according to

$$\delta E_d = E_{|D_{xx}, x\rangle} - E_{|D_{xx}, y\rangle} = E_{|D_{yy}, y\rangle} - E_{|D_{yy}, x\rangle} = 3\mathcal{E}. \quad (11)$$

Comparing Eqs. (10) and (11) we conclude that splittings of the ss - and pp -shells differ by 8β .

III. INTERPLAY BETWEEN EXCITON-Mn AND ELECTRON-HOLE EXCHANGE INTERACTION

The Hamiltonian describing exciton-Mn exchange interaction can be conveniently represented in the basis of the certain components s, j, M of the electron, hole and Mn-ion spins as

$$\mathcal{H}_{\text{Mn}} = [A_e s \delta(\mathbf{r}_0 - \mathbf{r}_e) + A_h j \delta(\mathbf{r}_0 - \mathbf{r}_h)] M, \quad (12)$$

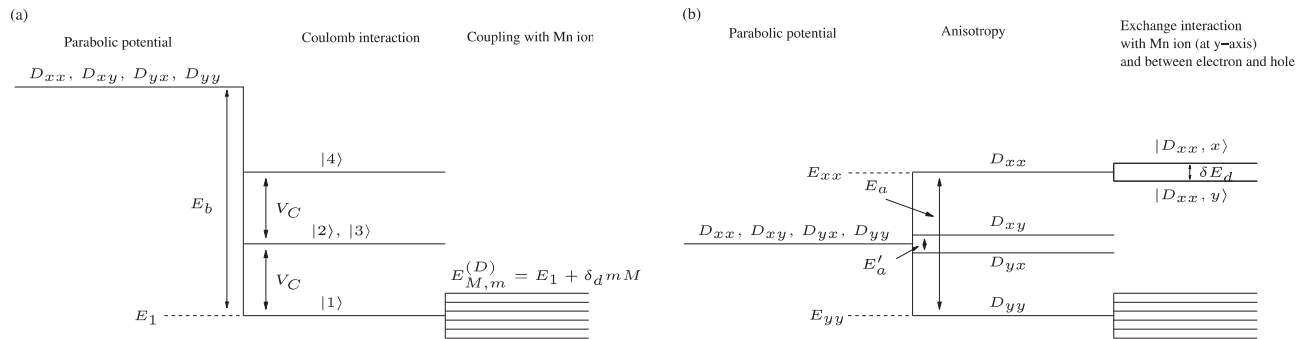


FIG. 1: Schematic pp -shell energy-level diagram for the axial (a) and anisotropic QD (b). The energy splittings are shown not to scale.

where \mathbf{r}_0 is the Mn ion position, A_e and A_h are the coupling parameters for conduction and valence band electrons.¹³ In derivation of Eq. (12) we took into account only $j = \pm 3/2$ hole states and neglected the interaction with the electron in-plane spin since, for the realistic set of parameters, $A_e < A_h/2$, see Refs. 3,10.

In a QD with an embedded Mn ion, fine structure of the ground-state exciton is determined by the interplay between the QD anisotropy and the exchange coupling with the Mn ion. From now on we consider the most important (from both experimental and theoretical points of view) case where the ground state anisotropic splitting Eq. (10) is negligible as compared with the coupling with a magnetic ion. Without the exciton-ion exchange interaction, the ground state of the system “exciton + Mn ion” is 4×6 -fold degenerate. The interaction \mathcal{H}_{Mn} splits this state into 12 doubly-degenerate sublevels half of which, namely, those with the exciton angular-momentum component $m \equiv s + j = \pm 1$, are optically active (or bright). Their energies are given by

$$E_{m,M}^{(S)} = E_0^{(S)} + \delta_s m M, \quad \delta_s = (3I_h^{(s)} - I_e^{(s)})/2, \quad (13)$$

where $E_0^{(S)}$ is the ss -shell exciton energy,

$$I_e^{(s)} = \frac{A_e}{\pi a_e^2} e^{-\rho_0^2/a_e^2} \varphi_{e1}^2(z_0), \quad I_h^{(s)} = \frac{A_h}{\pi a_h^2} e^{-\rho_0^2/a_h^2} \varphi_{hh1}^2(z_0),$$

$\rho_0^2 = x_0^2 + y_0^2$; x_0, y_0 and z_0 are the Cartesian components of \mathbf{r}_0 and the envelope $\varphi_{e1}(z)$ or $\varphi_{hh1}(z)$ describes the electron or hole confinement along z .

The fine structure of the pp -shell exciton excited states is determined by a combined effect of the exciton-Mn and the electron-hole (long-range) exchange interactions. If the QD anisotropy is small so that $|E_a| \ll V_C$ the only one bright state $|1\rangle$ defined by Eq. (3) splits into 6 doubly-degenerate sublevels, see Fig. 1a,

$$E_{m,M}^{(D)} = E_1 + \delta_d m M, \quad (14)$$

where E_1 is the energy of $|1\rangle$ state,

$$\delta_d = \frac{1}{2}(3I_h^{(d)} - I_e^{(d)}), \quad (15)$$

and the coupling constants

$$I_e^{(d)} = \frac{r_0^2}{a_e^2} I_e^{(s)}, \quad I_h^{(d)} = \frac{r_0^2}{a_h^2} I_h^{(s)}, \quad (16)$$

are strongly sensitive to the position of the Mn ion. For example, if the Mn ion is located exactly in the QD center the splitting of pp -shell states vanishes.

In highly anisotropic QDs where $V_C \ll E_a$ the fine structure of the D_{xx} and D_{yy} levels is even more rich. In general case an overlap between exciton and Mn ion is different for these two orbitals and one needs to introduce two coupling constants for each type of the carriers, namely,

$$I_e^{(xx)} = \frac{x_0^2}{a_e^2} I_e^{(s)}, \quad I_h^{(xx)} = \frac{x_0^2}{a_h^2} I_h^{(s)}, \quad (17)$$

$$I_e^{(yy)} = \frac{y_0^2}{a_e^2} I_e^{(s)}, \quad I_h^{(yy)} = \frac{y_0^2}{a_h^2} I_h^{(s)}.$$

The eigen energies are determined by the interplay of the exciton-Mn interaction described by the parameter

$$\delta_{ii} = 3I_h^{(ii)} - I_e^{(ii)} \quad (i = x, y), \quad (18)$$

and the long-range exchange splitting Eq. (11). For a fixed orbital D_{ii} one should observe six doubly-degenerated lines with energies

$$E_{m,M}^{(ii)} = E_{ii} \pm \sqrt{\left(\frac{\delta E_d}{2}\right)^2 + (\delta_{ii} M)^2}, \quad (19)$$

where E_{ii} is the position of the corresponding unperturbed orbital. For $E_d \neq 0$, the levels are nonequidistant and the crossover between anisotropy dominated regime with two linearly polarized states ($\delta E_d \gg \delta_{ii}$) and the regime of dominant exciton-Mn interaction ($\delta E_d \ll \delta_{ii}$) with six equidistant sublevels takes place.

IV. DISCUSSION AND COMPARISON WITH AN EXPERIMENT

We use micro-spectroscopy to analyze the optical properties of individual Mn-doped self-assembled CdTe/ZnTe

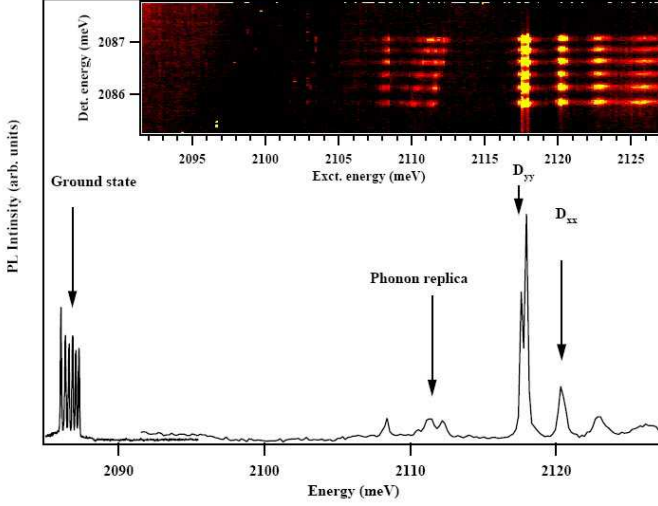


FIG. 2: (Color online) Experimental PL and PLE spectra of Mn-doped quantum dot exciton. The spectral features related to the ground and excited states are marked correspondingly. The inset shows the contour plot of the multi-channel PLE.

QDs. Single Mn atoms are introduced in CdTe/ZnTe QDs^{3,4,5} by adjusting, during the growth process, the density of Mn atoms to be roughly equal to the density of QDs.¹⁴ The PL of individual QDs is excited with a tunable dye laser and collected through aluminium shadow masks with $0.2 \dots 1.0 \mu\text{m}$ apertures. The PL is then dispersed by a 2-m additive double monochromator and detected by a nitrogen cooled Si charge-coupled device (CCD).

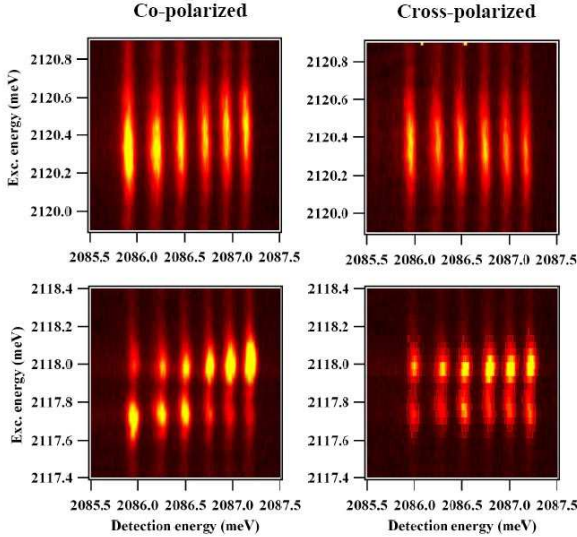


FIG. 3: (Color online) PLE contour plots for excited states D_{xx} (upper panel) and D_{yy} (lower panels) obtained for co-polarized (left panels) and cross-polarized (right panels) circular excitation.

The experimental findings for a Mn-doped QD are

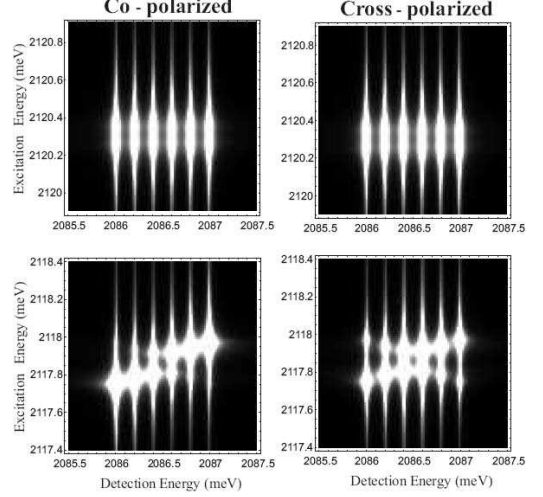


FIG. 4: Calculated PLE spectra in co-polarized (left) and cross-polarized (right) configuration. The parameters used are as follows: $E_{yy} = 2117.86 \text{ meV}$, $E_{xx} = 2120.30 \text{ meV}$, $\delta E_d = 0.05 \text{ meV}$, $\tilde{\delta}_{xx} = 0.01 \text{ meV}$, $\tilde{\delta}_{yy} = 0.04 \text{ meV}$, $\delta_s = 0.2 \text{ meV}$ and $E_0^{(S)} = 2086.5 \text{ meV}$. The lines are Lorentzian-broadened with the widths $\Gamma_s = 0.03 \text{ meV}$ and $\Gamma_{xx} = 0.06 \text{ meV}$, $\Gamma_{yy} = 0.03 \text{ meV}$.

summarized in Figs. 2, 3, and 5. This particular QD shows clear linearly polarized excited states. The analysis of the fine structure of other QDs presenting linearly polarized excited states leads qualitatively to the same conclusions. We also note that some QDs demonstrating the excited states in the same energy range present a very weak or non-detectable linear polarization splitting. Fig. 2 shows PL and PLE spectra of this QD. The ground state PL demonstrates 6 equidistant lines positioned at $\sim 2086 \text{ meV}$. These lines correspond to different projections of Mn spin (see Eq. (13)). Their approximately equal intensities and regular energy spacing evidence the negligible anisotropic splitting of the ground state. The splitting between these lines suggests the value $\delta_s \approx 0.2 \text{ meV}$ being in a good agreement with previous studies.³

The first absorption lines in the measured PLE (Fig. 2) lie by $\sim 25 \text{ meV}$ above the ground state. This energy range corresponds to the LO-phonon energy between CdTe and ZnTe, thus this feature can be identified with the phonon replica of the ground state. The non-trivial PLE pattern coming from the replica is a consequence of complicated phonon spectra in such QDs system.

Now we proceed with the discussion of the excited-states fine structure. Two excited states with energies $\approx 2117.86 \text{ meV}$ and 2120.30 meV are seen in Fig. 2. We relate them with the D_{yy} - and D_{xx} -orbital states. The difference in their intensities can be attributed to (i) the shorter lifetime of the highest energy state and (ii) the Coulomb interaction which, according to Eqs. (3) and (4), intermixes the D_{xx} and D_{yy} states. The latter effect reduces the oscillator strength of the higher state and, as

a result, the anisotropic exchange splitting of this state.

A value of the ratio between the energy separation of the excited states D_{xx} and D_{yy} and the distance between ground and excited states allows one to estimate from Eq. (6) the quantum dot anisotropy degree β to be ≈ 0.02 which supports the assumption that the anisotropic splitting of ss -shell state is not observed. Figure 2 clearly manifests the splitting of D_{yy} state into a pair of lines. We assume this splitting to come from the QD anisotropy [see Eq. (11)]. The splitting of D_{xx} state is not observed for the reasons suggested above.

The comparison between the experimental data and theoretical predictions in Figs. 3 and 4, respectively, shows that the best possible agreement of the data is obtained for anisotropic splitting $\delta E_d = 0.05$ meV and $\tilde{\delta}_{yy} = 0.04$ meV. The order of magnitude of δE_d is consistent with the quantum dot size $a_e = 45$ Å and $a_h = 90$ Å (i.e. $\zeta = 2$). It agrees with other results for II-VI QDs where the hole confinement is weaker than that of electrons.¹⁵ For these parameters the predicted energy separation between the ground and excited states is 43 meV which is somewhat larger than the experimentally observed 33 meV.

Fully quantitative description of the experimental results would require a more complicated theory taking into account all details of the band structure and confinement potential as well as the short-range contribution to the exchange interaction.^{16,17}

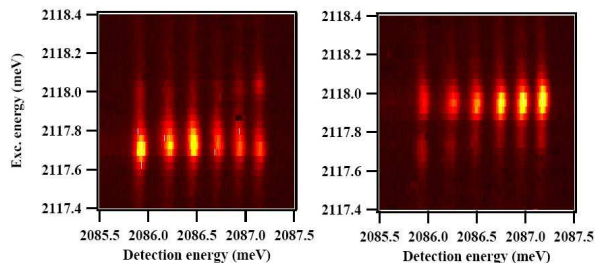


FIG. 5: (Color online) PLE spectra of D_{yy} states for linearly polarized excitation and unpolarized detection. Left and right panels correspond to two orthogonal linearly polarized excitations.

In order to have a deeper insight into the fine structure of the D_{yy} state we have performed the PLE measurements for the linearly polarized excitation and unpolarized detection. The experimental results are given in Fig. 5. The theoretical PLE plots calculated for the same parameters as the spectra for circularly-polarized excitation are shown in Fig. 6. The reasonable agreement between the theory and experiment is seen. We note that we do not introduce any spin relaxation in the calculations. The similarity in the PL intensity distribution obtained in the theory and in the experiment shows that under resonant excitation the spin relaxation time of the exciton-Mn complex is much more longer than the life-

time of the exciton: no significant relaxation occurs dur-

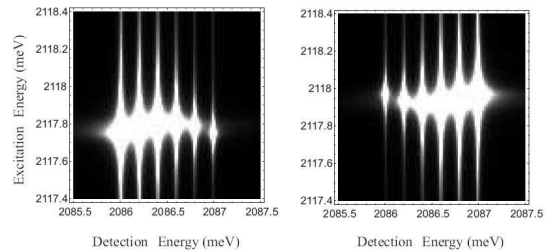


FIG. 6: Calculated PLE spectra for linearly polarized excitation and unpolarized detection. Left and right panels correspond to two orthogonal linear polarizations. The parameters used in the calculation are given in the caption of Fig. 4

ing the exciton lifetime. As shown in Figs. 3 and 5, this long spin relaxation time combined with the fine structure of the excited states permits to create selectively a given spin configuration of the exciton-Mn complex by tuning the polarization and wavelength of the excitation laser.

Let us note finally that the experimentally observed PLE intensity distribution for the higher energy state D_{xx} is almost uniform, therefore we conclude that the exciton-Mn ion coupling is smaller for this state as compared to D_{yy} . We can thus conclude that the Mn ion is located nearby the y axis. If we completely neglect electron-Mn interaction, using Eq. (18) and the fitted value $\tilde{\delta}_{yy} = 0.04$ meV we deduce that the Mn-ion is positioned at $y_0 \approx 0.3a_h$, $x_0 \ll y_0$.

V. CONCLUSION

In conclusion, we have performed a combined experimental and theoretical study of the fine structure of exciton excited states in the QDs containing a single magnetic ion. We have identified two regimes of uniaxial and anisotropic quantum dots where the qualitatively different level arrangement and PLE spectra are predicted. The theoretical results are compared with the experimental data on photoluminescence and photoluminescence excitation for an individual Mn-doped QD. All important experimental observations are reproduced theoretically. The comparison has made possible to determine the Mn-exciton interaction constants, QD anisotropy degree and to estimate the position of the Mn ion in the quantum dot.

Acknowledgments

The work was partially supported by RFBR, “Dynasty” foundation – ICFPM and French ANR contract MOMES.

-
- ¹ G. Bacher, A.A. Maksimov, H. Schmig, V.D. Kulakovskii, M.K. Welsch, A. Forchel, P.S. Dorozhkin, A.V. Chernenko, S. Lee, M. Dobrowolska, J.K. Furdyna, Phys. Rev. Lett **89**, 127201 (2002).
- ² S. Mackowski, T. Gurung, H.E. Jackson, L.M. Smith, G. Karczewski, J. Kossut, Appl. Phys. Lett. **87**, 072502 (2005).
- ³ L. Besombes, Y. Léger, L. Maingault, D. Ferrand, H. Mariette and J. Cibert, Phys. Rev. Lett. **93**, 207403 (2004).
- ⁴ L. Besombes, Y. Léger, L. Maingault, D. Ferrand, H. Mariette and J. Cibert, Phys. Rev. B **71**, 161307(R) (2005).
- ⁵ Y. Léger, L. Besombes, L. Maingault, D. Ferrand and H. Mariette, Phys. Rev. Lett. **95**, 047403 (2005).
- ⁶ Y. Léger, L. Besombes, L. Maingault, D. Ferrand and H. Mariette, Phys. Rev. B **72**, 241309(R) (2005).
- ⁷ Y. Léger, L. Besombes, J. Fernández-Rossier, L. Maingault and H. Mariette, Phys. Rev. Lett. **97**, 107401 (2006).
- ⁸ F. Qu, P. Hawrylak, Phys. Rev. Lett. **96**, 157201 (2006).
- ⁹ A.O. Govorov, Phys. Rev. B **70**, 035321 (2004).
- ¹⁰ J. Fernández-Rossier, Phys. Rev. B **73**, 045301 (2006).
- ¹¹ Al. L. Efros and M. Rosen, Phys. Rev. B, **58**, 7120 (1998).
- ¹² M. M. Glazov, E. L. Ivchenko, R. v. Baltz, and E. G. Tsitsishvili, Int. J. Nanosci., 2006, cond-mat/0501635.
- ¹³ I. A. Merkulov, D. R. Yakovlev, A. Keller, W. Ossau, J. Geurts, A. Waag, G. Landwehr, G. Karczewski, T. Wojtowicz, and J. Kossut, Phys. Rev. Lett. **83**, 1431 (1999).
- ¹⁴ L. Maingault, L. Besombes, Y. Leger and H. Mariette, Appl. Phys. Lett. **89**, 193109 (2006)
- ¹⁵ B. P. Zhang, W. X. Wang, T. Yasuda, Y. Segawa, K. Edamatsu, and T. Itoh, Appl. Phys. Lett. **71**, 3370 (1997).
- ¹⁶ I.L. Aleiner and E.L. Ivchenko. Pis'ma Zh. Exper. Teor. Fiz **55**, 662 (1992).
- ¹⁷ Alberto Franceschetti and Alex Zunger, Phys. Rev. Lett. **78**, 915 (1997).
- ¹⁸ We note that for p -shell excited states the Coulomb interaction is the same for P_x and P_y states and therefore, in the axial approximation, and the fine sublevels of p -shell are split due to long-range exchange only, see Ref. 12